



## Turbine Type Rotary Wave Energy Converter Performance

Perihan KARAKOSE<sup>1,\*</sup> , Ahmet KOCA<sup>2</sup> 

<sup>1</sup>Bartın University, Electronic and Automation Department, 74100, Bartın, Turkey

<sup>2</sup>Firat University, Mechatronic Engineering Department, 23100, Elazığ, Turkey

### Highlights

- Numerical wave generated using Ansys VOF model.
- Six-dof rotation of the turbine with the effect of the wave.
- Observation of the dynamic parameters acting on the turbine depending on the different wave forms.

### Article Info

Received: 10 Aug 2022

Accepted: 24 Apr 2023

### Keywords

Wave energy  
Dynamic mesh  
VoF method  
Rotating turbine

### Abstract

In this investigation, the utilization of water waves as the fluid medium is explored in the context of turbines, which are mechanical devices that convert fluid motion into rotational motion. The Volume of Fluid (VOF) model in Ansys Fluent is employed to generate regular waves and analyze the turbine's movement in a wave tank. Essential parameters such as force, pressure, momentum, and speed of the turbine are investigated to harvest electrical energy from wave energy. The study aimed to understand how these parameters changed with varying wave characteristics. Results showed that dynamic pressure and moment increase as the wavelength increased. However, the turbine's rotation speed decrease as wavelength increased. The force acting on the blades do not change significantly with wavelength but caused a time delay. The highest force applied to the turbine blades is observed at a wave height of 2 m, reaching 8000 N. Finally, the maximum turbine speed is attained at a wave height of 2 m and wave period of 7 s, reaching 87 mm/s. However, the maximum efficiency of 19.18% is achieved at a wave height of 1m and a wave period of 8.75 seconds. Because as the wave height increases, the power of the wave increases significantly, but the absorption of this power increases at a lower rate. Therefore, this study highlights the need to increase the number of wave energy conversion systems that can operate efficiently for wave forms with high wave heights.

## 1. INTRODUCTION

Fossil fuels are depleting rapidly due to developing technology, climate change, global warming and population growth. An estimated 90% of energy needs in the world are obtained from fossil fuels. Therefore, the demand for renewable energy increase day by day. Wave, wind, solar, geothermal and hydraulic energy resources are widely used renewable energy sources. Wave energy has a very high energy potential. The efficiency of wave energy converter systems varies between 10% and 40% depending on the wave parameters [1] Wave power plants have high establishment and operation cost [2]. For Wave Energy Converter systems(WECs)., wave parameters are critical. Therefore, in this study, the effects of wave parameters on the turbine were investigated numerically. In the studies, the similarity of the experimentally obtained waves with the Ansys VOF model has been confirmed. For this reason, regular waves are obtained by using the Ansys VOF model in this study.

Studies on simulating ocean waves have increased recently. Because the experimental WEC model requires a high installation cost. Wave models in nature cannot be expressed mathematically. However, an attempt has been made to define waveforms with various approaches in order to use them in calculations. All waves in a wave group must conform to the mathematically expressed form of the wave equation. In any case, this dependency depends on the boundary conditions. These boundary conditions can be defined as linear or nonlinear. Zhi and Zhan [3] are modeled the cnoidal wave model, which is a nonlinear wave model, using

\*Corresponding author, e-mail: perihan.karakose1@gmail.com

the ansys VOF package. Finnegan and Goggins [4] are modeled the linear wave model in ANSYS. Zhu et al. [5] used Reynolds-Averaged Navier Stokes(RANS) equations in NWT modeling. In addition, the momentum source is added as User Defined Functions (UDF) to create regions under the effect of different motions and forces in the simulation. The breakwater's response to generated waves is studied both mathematically and empirically. A kinematic analysis of the extreme wave model utilizing RANS is studied by Oijeh et al. [6] With the use of RANS and VoF simulations, they generate both regular and irregular waves on the sea's surface.

Flap type [7, 8] and piston type [9, 10] wave makers are commonly used to create waves. Yamac and Koca [11] have moved the wall using UDF in Ansys in order to generate waves. The waves created by these methods can be reflected back if the wave tank is not long enough. Yamaç and Koca [12] modeled a wave tank with a length of 400 m for the 9s period and 111.4 m for the 6s wave period to avoid back reflection. This increases the size of the mesh in the wave tank. This causes a significant increase in the computation time. Liu et al. [13] apply the porous structure to the wall opposite the wavemaker so that the waves do not reflect from the end of the tank. However, in this study, Ansys beach module is actively used to avoid reflection of the wave.

Using NWT analysis, Bhinder et al. [14] looked into the impact of fluid forces on WECs systems. An analysis is done on the relationship between system efficiency and the forces exerted on the system. Yamac and Koca [15] studied the water rise in the OWC due to the wave in the NWT. The results show that the water rises even in the 8 m high wave tank. Koca et al. [16] studied the increase in elevation in the OWC using an inclined wave tank. It has been stated that the decrease in the ratio of the tank length to the sloped floor projection increases the output power. Anbarsooz et al. [17] modeled the two-dimensional wave tank with the VOF technique using Ansys Fluent 15.0. The Oscillating Water Column (OWC) WEC is investigated using the wave tank. In the simulations, the  $H/L$  ratio was fixed at 0.069.  $H$  is the wave height, and  $L$  gives the wavelength. The results showed that the increase in wave height reduces the wave absorption performance of OWC. Gomes et al. [18] optimized OWC's geometric parameters using the two-dimensional wave tank in Ansys Fluent. The mass flow rate, pressure, power and efficiency values are observed in the height to length ratio of OWC ( $H/L$ ). In the results, the maximum efficiency (40%) is obtained by fixing the  $H/L$  ratio to 0.13. Therefore, in this study, the  $H/L$  ratio is taken as 0.13. Morris et al. [19] modeled turbine designs used for underwater flow in Ansys Fluent. Turbines are deformed with the effect of hydrodynamic forces underwater. In their study, shaft power, blade tip displacement and displacement by axial thrust are investigated for 2, 3 and 4 blade rotor configurations. Deformation of 2, 3 and 4 blade rotors are reduced based on solid-liquid interaction model data. For this reason, in this study, the forces acting on a turbine fixed axially on the water are investigated. It would be appropriate to use this turbine for systems that have low deformation rate and can generate electricity continuously, as a result of fixing this turbine to floating vehicles such as ships. Sarma et al. [20] experimentally and numerically study the performance of the savonius rotor in the wave tank. The study gives water velocity between 0.3 and 0.9 m / sec. The savonius rotor used in the wave tank provided a more stable rotation and is expected to have a longer life. In this study, only the speed of the savonius rotor is considered. However, for the electrical energy it can produce. The dynamic effects are examined. Kumar et al. [21] investigated the effect of blade angle and blade shape factor of savonius rotor on power factor. The water speed in the channel is given between 0.5 and 2 m / sec. The blade shape factor is the blade length ratio to the diameter of the blade curvature ( $p/q$ ). 4 different values between 0 and 0.6 are taken as the blade shape factor. 4 different values between  $110^\circ$  and  $150^\circ$  are taken for the blade angle. In the results, the maximum power factor in water with a velocity of 2 m / s is obtained as 0.426. The result is obtained with a blade shape factor of 0.6 at a blade angle of  $150^\circ$ . Elbatran et al. [22] placed the savonius rotor in an extended channel for low speed regions. In this study, channels with 6 different geometric shapes are tested. In the results, it is observed that this channel increased the maximum power factor by 78%. For lakes and waterways, this approach works well. A turbine is typically used to harness the flow created by tidal events in the ocean. However, the efficiency of the turbines decreases as the flow direction changes. Therefore, Bai et al. [23] proposed a three turbine approach with a triangular position. In the study, the angle of this triangular structure and the distance between the turbines are changed, and the most suitable structure is determined numerically. The power output is obtained from this suitable value design increased 6% compared to the uniform turbine. In addition, the effect of the change in the flow direction decreased compared to a uniform turbine structure.

In this study, the 3D wave tank is modeled in Ansys Fluent, and the motion of the turbine in the wave tank is investigated. The turbine's force, moment and dynamic pressure values are examined depending on the wave parameter. The remainder of the paper is organized as follows: Section 2 introduces problem formulation and boundary conditions in Ansys Fluent. This section presents the mesh structure and waveforms from the wave tank. Section 3 investigates moment, force, dynamic pressure and turbine speed on the turbine. Finally, conclusions are summarized in section 4.

## 2. MATERIAL AND METHODS

This section involves the creation of an NWT model using the ANSYS program to simulate real waves. Furthermore, the study investigates the dynamic impact of water waves on a turbine by placing the turbine on the water surface.

### 2.1. Governing Equations and Boundary Conditions

The focus of this study is on the simulation of regular gravitational waves, which are surface waves characterized by two primary parameters: wave height and wave period. Two different theories are used to explain gravitational waves. Linear Wave Theory is used for waves with small amplitudes and lengths, whereas the quadratic Nonlinear Stokes equation is employed for waves with high amplitudes and long wavelengths.

As per McCornick's findings [24], the waves that form on the free surface of the water are in a state of equilibrium. When an object is dropped into a tank of water, an irregularity occurs, which leads to the formation of surface waves. However, due to the force of gravity, the water tends to return to its natural state of equilibrium, thereby creating what are referred to as gravitational waves. In contrast, Dean and Darlymple posit that waves come in various shapes and sizes, depending on factors such as wind direction and forces acting on the water [25].

The parameters characterizing a simple wave can be described by Equation (1). The variables "H" and "h" respectively represent the water depth and wave height, "L" denotes the wavelength, "g" represents the acceleration due to gravity, "A" stands for the wave amplitude, and "T" denotes the wave period [12]

$$L = \frac{gT^2}{2\pi} \tanh \frac{2\pi h}{L}. \quad (1)$$

The power of a wave can be determined using Equation (2). On the other hand, Equation (3) provides the mechanical power of a turbine, where, " $T_0$ " is torque value and "W" is turbine velocity

$$P = \frac{\rho g^2}{64\pi} h^2 T \left( \frac{kW}{m} \right) \quad (2)$$

$$P_0 = \frac{T_0}{w}. \quad (3)$$

The development of waves is influenced by both linear and non-linear factors, which are dependent on the boundary conditions and physical environment. Gravitational waves are subject to three distinct boundary conditions, as noted in [12].

The kinematic water surface boundary condition stipulates that the fluid cannot be detached from the free surface of the water. Moreover, the normal fluid velocity at each point on the water surface is equivalent to the normal velocity of the surface. This condition is represented by Equation (4), where " $Z = \eta$ " denotes that the particle velocity is equal to the normal velocity of the water surface

$$V|_{z=\mu} \approx \frac{\partial n}{\partial t} k_b = \frac{\partial \varphi}{\partial t} |_{z=0} k_b. \quad (4)$$

" $\phi$ " is the potential function, " $k_b$ " is the average unit vector, " $V$ " is the velocity.

The dynamic water surface boundary condition dictates that a water particle on the surface of the water follows circular or elliptical trajectories based on the water depth during vertical displacement indicated by the variable " $\eta$ ." The pressure at the surface of the water must be zero at any given position " $x$ " and time " $t$ ." This condition is incorporated into Equation (5) by applying the Bernoulli equation to the surface of the water

$$\frac{\partial \phi}{\partial t} + gn + \frac{1}{2}V^2 = 0. \quad (5)$$

In the case of waves, the fluid motion is continuous, allowing the continuity equation to be utilized. In situations where the flow is irregular, its velocity can be expressed as a potential function. Equation (6) represents the continuity equation

$$\nabla^2 \phi = 0. \quad (6)$$

The velocity satisfying the boundary conditions is given in Equation (7)

$$\phi = \frac{\alpha G \cosh [k(z+h)]}{w \cosh [(kh)]} + \sec(kx - wt) \quad (7)$$

" $w$ " is wave frequency, " $k$ " is wave number, " $t$ " is time. " $w = 2\pi / T$ " is " $k = 2\pi / L$ ". The mathematical formula for the velocity components is obtained from Equations (8)- (9)

$$u = \frac{\partial \phi}{\partial x} = \frac{agk \cosh [k(z+h)]}{w \cosh [(kh)]} + \cos(kx - wt) \quad (8)$$

$$a = \frac{\partial \phi}{\partial z} = \frac{agk \operatorname{sech} [k(z+h)]}{w \cosh [(kh)]} + \sec(kx - wt). \quad (9)$$

In the context of surface waves, the velocity component in the horizontal ( $x$ ) direction is denoted by " $u$ ," while the velocity component in the vertical ( $z$ ) direction is denoted by " $w$ ." The equation that defines the motion of the surface is shown in Equation (10)

$$\eta = A \cos(kx - wt). \quad (10)$$

Stokes' theory describes wave motion properties as a series of minor irregularities that depend on the wave velocity potential [25]. Both Linear Wave Theory and Stokes' Theory can be applied to deep waters and high wavelengths. The velocity potentials, as given in Equation (11), are expressed in the Stokes equation as power series

$$\phi = \epsilon \phi_1 + \epsilon^2 \phi_2 + \epsilon^3 \phi_3 \dots \quad (11)$$

" $\epsilon$ " is the power series variable. The solution with the first-order term " $\phi_1$ " represents the linear theory. The expansion of the second term " $\phi_2$ " represents the Stokes quadratic equation.

The orbital movements of waves are characterized by a non-linear structure, as they do not conform to a closed cycle. The behavior of waves is further influenced by ocean currents, which create mass transfer in the direction of the waveform, adding to its non-linear nature. The motion of the free surface can be described using the Stokes quadratic equation, as shown in Equation (12) [24, 25]. The velocity components are expressed in Equations (13) - (14), where " $Z$ " represents the displacement of the free water surface with respect to the sea bed

$$\eta = A \cos(kx - wt) + \dots + \frac{A^2 k \cosh(kh)}{4 \operatorname{sech}^3(kh)} [2 + \cosh(2kh)] \cos 2(kx - wt) \quad (12)$$

$$u = Agk \frac{\cosh[k(z+h)]}{w \cosh(kh)} \cos(kx - wt) + A^2 wk \frac{\cosh 2k(k+z)}{\operatorname{sech}^4(kh)} \cos 2(kx - wt) \quad (13)$$

$$w = Agk \frac{\operatorname{sech}[k(z+h)]}{w \operatorname{sech}(kh)} \sec(kx - wt) + A^2 wk \frac{\operatorname{sech} 2k(k+z)}{\cos^4(kh)} \sec 2(kx - wt) . \quad (14)$$

Open channel wave boundary conditions are used in the marine industry to generate regular/irregular waves necessary to analyze wave kinematics and wave impact loads on moving hulls and offshore structures. Small amplitude wave theories are generally applicable for low wave steepness and low relative height. However, finite-amplitude wave theories are more suitable for high wave steepness or high relative height. Wave steepness is generally defined as the ratio of wave height to wavelength and relative height as the ratio of wave height to water depth. Short gravitational wave expressions for each wave theory are expressed in infinite fluid height, shallow or transitional wave expressions are expressed in finite fluid height. The wavenumber  $k$  is given in Equation (15).  $\lambda$  represents the wavelength

$$k = \frac{2\pi}{\lambda} . \quad (15)$$

The equation for wave velocity is shown in Equation (16), where 'c' represents the velocity of the wave. The frequency of the wave is denoted by 'W'. In Ansys Fluent, the calculation of wave velocity depends on the defined wavelength and wave height in the system

$$c = \frac{w}{k} . \quad (16)$$

## 2.2. Computational Domain and Mesh Structure

The VOF method is commonly used in time-dependent solutions in the Ansys Fluent package to model multiple incompressible fluids. It involves defining a volume fraction variable for each phase in computational cells, with different values assigned in different regions for each phase. Properties and variables in the cells are represented as a single-phase or mixture.

In this study, a three-dimensional wave tank simulation was conducted using the Fluent module, with half of the cubic geometry defined as the air phase and the other half as the water phase. The turbine was positioned on the water phase, and waves were generated using the Volume of Fluid method. Wave height and wavelength were introduced to the system using the VoF module in Fluent. An isometric view of the turbine positioned in the wave tank is shown in Figure 1. (a), with the wave tank having dimensions of 36 \* 20 \* 2 m.

Regular waves were obtained in the simulation with high wave heights, and it was determined that water depth plays an important role in regular wave simulation. Therefore, a water depth of 18 m was chosen, and the top 18 m of the wave tank was defined as the air phase. The beach module in Ansys was activated to prevent wave reflection, and a cavity was placed at the front and back of the turbine to prevent friction. The dimensions of the turbine are given in m in Figure 1. (b).

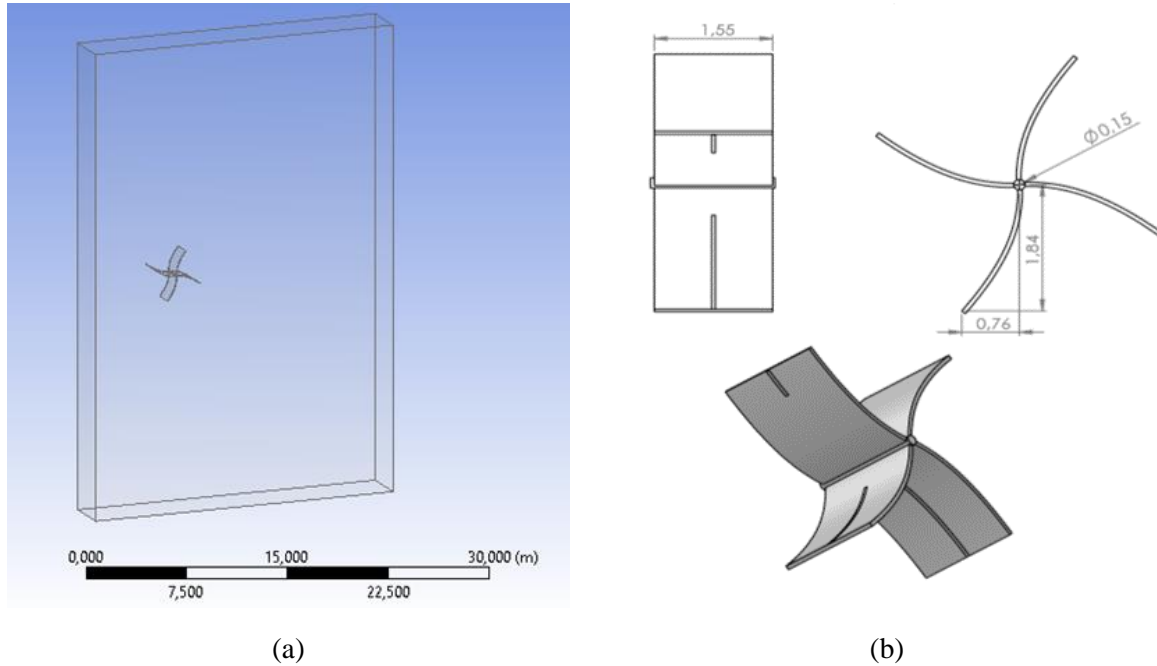


**Figure 1.** Turbine in the wave tank a) Isometric view of wave tank b) Dimensions of turbine

Figure 2 shows the finite volume mesh structure used in this study. The mesh contains a total of 156974 nodes and 880781 elements.

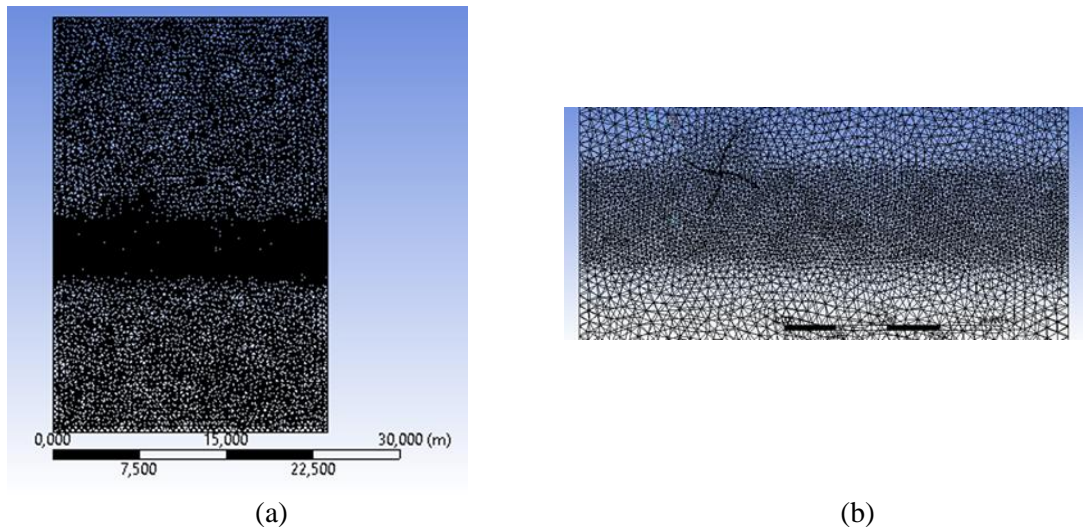


**Figure 2.** Mesh structure a) Mesh structure of wave tank b) Mesh structure of the turbine

The dynamic mesh model in Ansys Fluent is capable of modeling the motion of objects in single or multiphase flows. It automatically updates the volume mesh structure based on the new positions of the boundaries. ANSYS Fluent offers the use of limit profiles, user-defined functions (UDFs), and six degrees of freedom solvers for defining motion. Equation (17) represents the convection equation that describes the boundaries changing in coordinates

$$\frac{d}{dt} \int p\varphi dV + \int p\varphi (\bar{u} - \bar{u}_g) d\bar{A} = \int \Gamma \nabla_{\varphi} d\bar{A} + \int S_{\varphi} dV \quad (17)$$

where  $p$  is water density,  $(\bar{u})$  is flow velocity,  $(\bar{u}_g)$  is mesh speed in the moving part,  $s_{\varphi}$  is diffusion coefficient,  $\varphi$  is source term.

The movement of dynamic parts can be defined in three ways: stationary, rigid body, and deforming. In this study, the front and back planes of the wave tank are deforming, while the turbine is considered a rigid body. An important aspect of dynamic mesh settings is the updating parameters of the mesh structure, which can be achieved through layering, remeshing, or smoothing.

Layering is useful for hexahedral mesh structures, where the model is divided into small squares that can be interchanged with a mesh structure. Remeshing is used for tetrahedral elements and is necessary when border displacement is large compared to natural cell sizes, which can cause cell quality to deteriorate or degenerate. If enacted cells are invalid, ANSYS Fluent collects and removes them locally. If new cells or faces meet the distortion criteria, the mesh structure is updated locally, otherwise new cells are discarded and old cells are preserved.

Smoothing is used to divide the moving surface mesh according to the velocity profile. In this study, remeshing and smoothing methods are employed in the dynamic mesh model to achieve turbine motion. By using these methods, the numerical simulations are expected to achieve reliable results that can be compared to experimental or analytical data in the literature.

### 2.3. Wave Models Validation

To ensure the reliability of numerical studies, they are often compared with experimental, analytical, or previously published results. In this study, the numerical wave elevation is compared with an analytical sinusoidal wave. Figure 3 presents the comparison between the numerical and analytical wave elevations at a wave height of 1.5 m and a wavelength of 20 m. Initially, there is some discrepancy between the analytical and numerical waves. However, after 5 seconds, the error is significantly reduced. Therefore, the turbine is placed 5 m beyond the breakwater to avoid the initial wave disturbance.

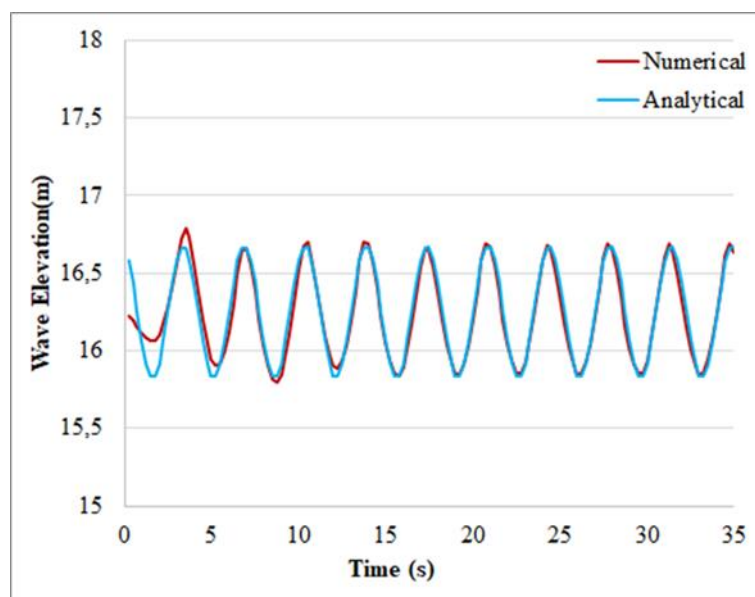
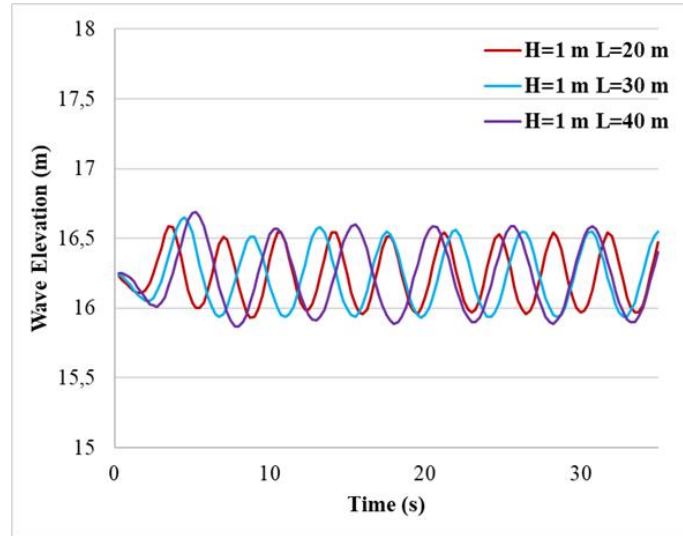
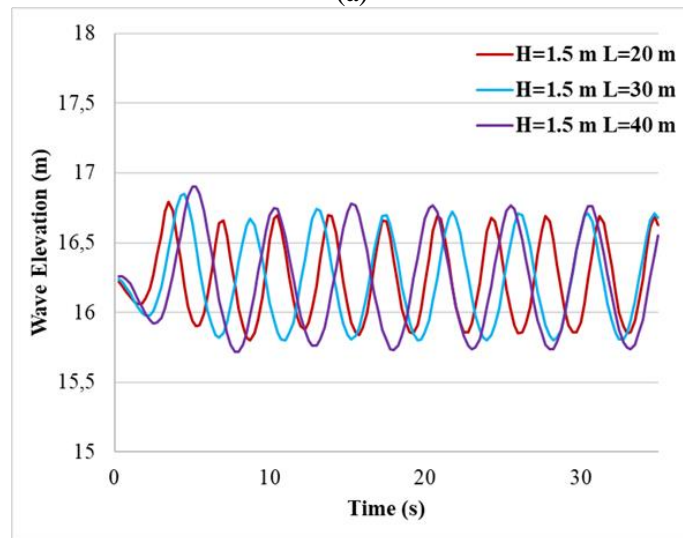


*Figure 3. Time-dependent wave elevation for validation*

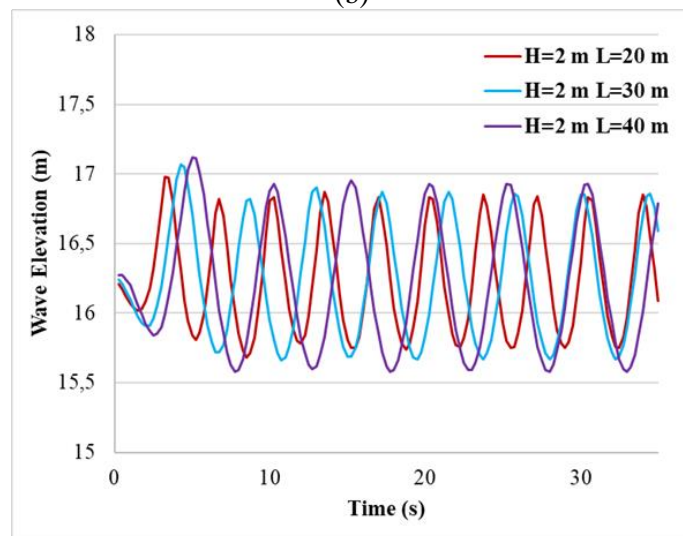
In this study, a numerical wave tank is used with dimensions of 20 m in length and 36 m in height. The tank is divided in half, with one half being the water phase and the other half being the air phase. The results are obtained at a location 5 m from the left side of the tank. Wave heights of 1 m, 1.5 m, and 2 m are tested, along with wavelengths of 20 m, 30 m, and 40 m. Figure 4 displays the water level at wave heights of 0.57 m, 0.85 m, and 1.1 m, showing a regular wave. However, the wave period is observed to be 7 s, 8.75 s, and 10 s, respectively, for each fixed wave height.



(a)



(b)



(c)

**Figure 4.** Wave elevation change with time a) Wave Height ( $H$ ) is 1 m, and wavelengths ( $L$ ) are 20 m, 30 m and 40 m s b) Wave Height ( $H$ ) is 1.5 m and wavelengths ( $L$ ) are 20 m, 30 m and 40 m c) Wave Height ( $H$ ) is 2 m, and wavelengths ( $L$ ) are 20 m, 30 m and 40 m

### 3. THE RESEARCH FINDINGS AND DISCUSSIONS

#### 3.1. Wave Models

This study investigates the impact of a water wave on turbines, which are often employed to generate mechanical motion from fluid motion. Various parameters such as force, momentum, turbine speed, and dynamic pressure are analyzed on the turbine blades as the wave affects them. The turbine is positioned 1.5 m above the water surface. Figure 5 illustrates the initial position of the wave tank and turbine.

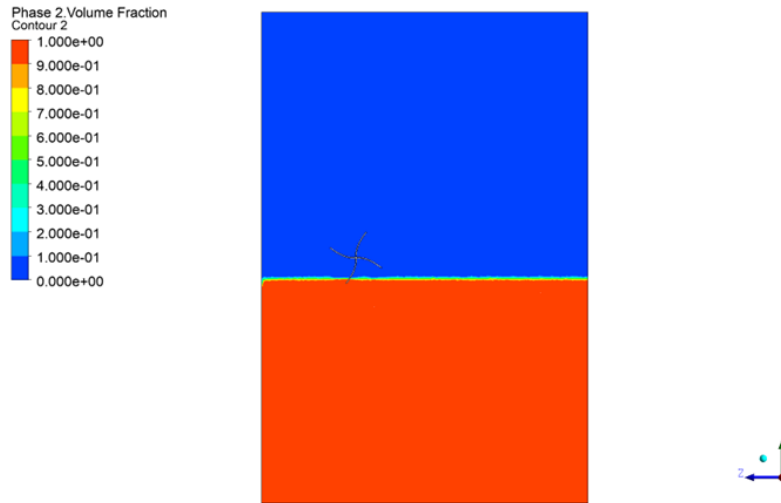


Figure 5. Position of wave tank and turbine at time  $t = 0$

In Figure 6, the movement of the turbine under the effect of the wave is shown for a period of 1 second. The turbine reaches a displacement of approximately 45 degrees at 3 seconds.

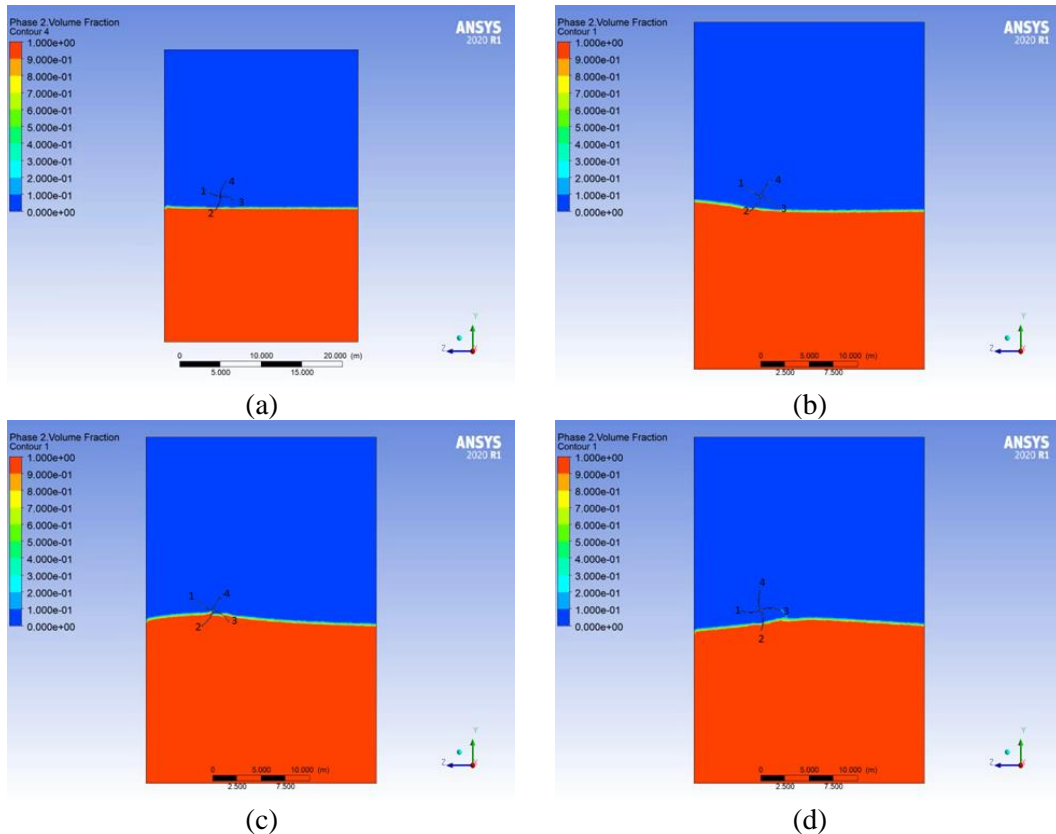


Figure 6. Movement of the turbine in water tank a)  $t=0$  s b)  $t=1$  s c)  $t=3$  s d)  $t=4$  s

The figure (Figure 7) displays the absolute pressure of the water and air phases in the wave tank. The pressure value reaches its maximum at the lowest point of the water phase, which is 16150 Pa. However, the pressure decreases as the water mass decreases from the lowest point to the upper point of the wave tank.

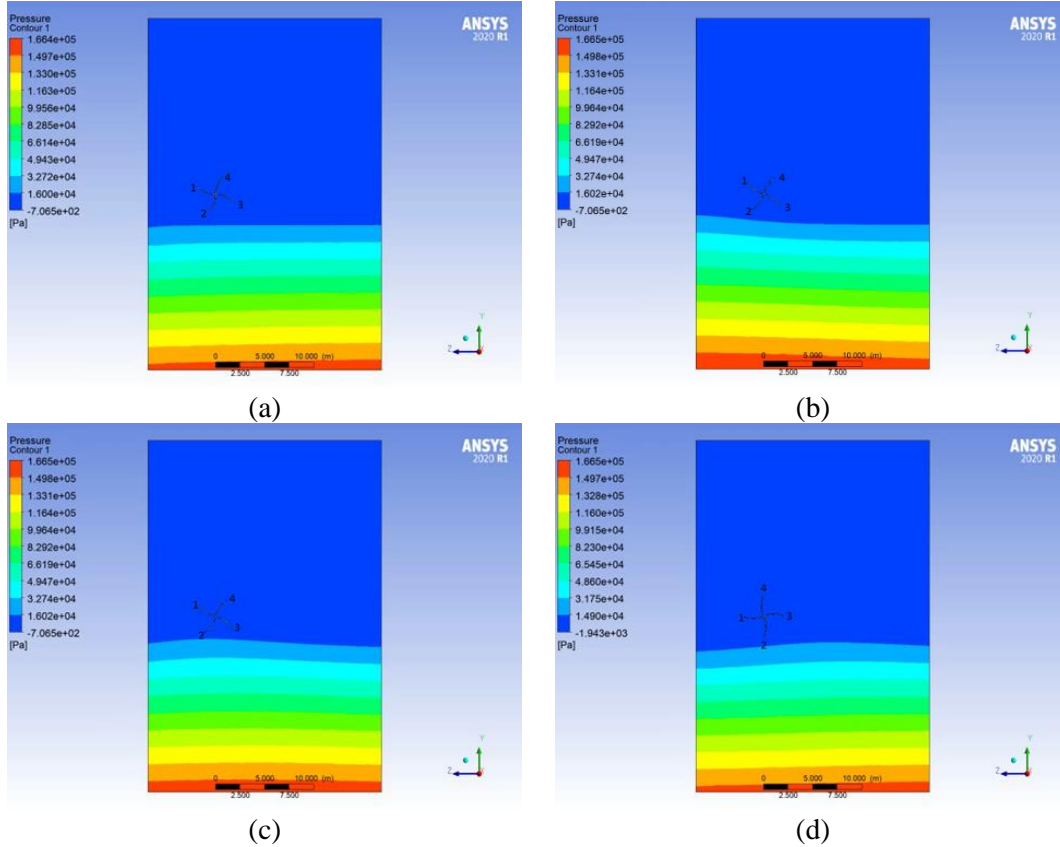
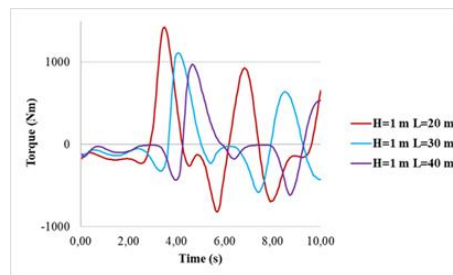


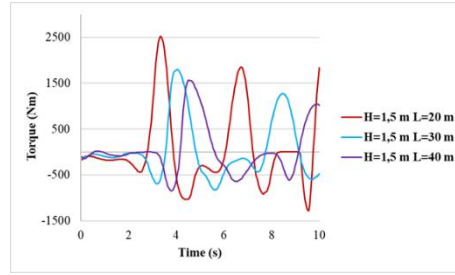
Figure 7. Absolute pressure change for 3 s a)  $t=0$  s b)  $t=1$  s c)  $t=3$  s d)  $t=4$  s

### 3.2. Investigation of the Effect of Regular Wave Motion on the Turbine

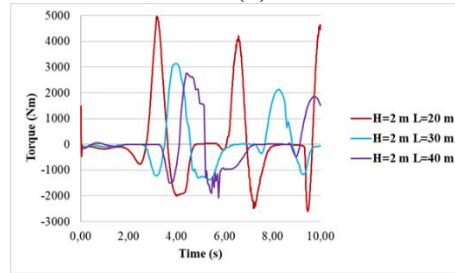
Figure 8 illustrates the variation of moment value over a duration of 10 seconds depending on the wave. Figure 8. (a) represents the moment values at fixed wavelengths of 20 m, 30 m, and 40 m with a wave height of 1 m. The figure indicates that the maximum moment value is observed at a wavelength of 20 m and reaches 1107.88 Nm. As the wavelength increases, the wave period also increases. The period is 7 s for 20 m wavelength, 8.75 s for 30 m wavelength, and 10 s for 40 m wavelength. The moment value and waveform change simultaneously with the periods. Hence, the moment value completes one cycle in 7 seconds at a wavelength of 20 m. Consequently, a phase angle occurs in the moment change at 20 m, 30 m, and 40 m wavelengths. The phase angle is illustrated in Figure 8. (a), (b), and (c). Furthermore, the moment value in the turbine blades increases with the wave height in Figure 8. (a), (b), and (c).



(a)



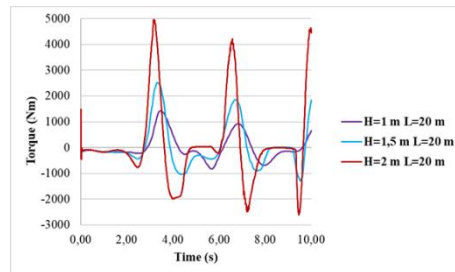
(b)



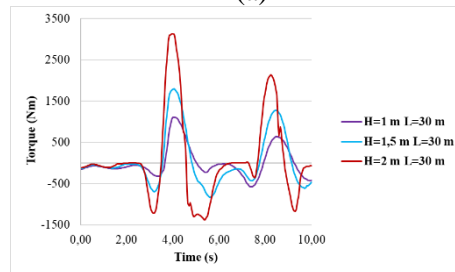
(c)

**Figure 8.** Torque value on turbine blades due to time-dependent wave at fixed a) Wave height ( $H$ ) is 1 m, and wavelengths ( $L$ ) are 20 m, 30 m and 40 m b) Wave height ( $H$ ) is 1.5 m and wavelengths ( $L$ ) is 20 m, 30 m and 40 m c) Wave height ( $H$ ) is 2 m, and wavelengths ( $L$ ) are 20 m, 30 m and 40 m

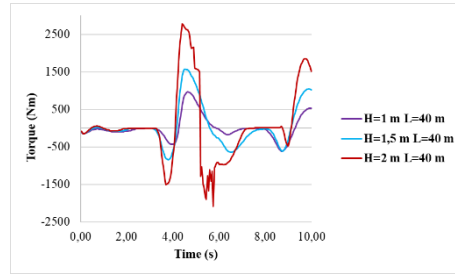
Figures 9.(a), 9.(b), and 9.(c) show the variation of the moment value of the turbine blades at fixed wavelengths with different wave heights. The moment value changes in the same period as the wavelength. Moreover, the moment value increases as the wave height increases in all three wavelengths in the turbine blades.



(a)



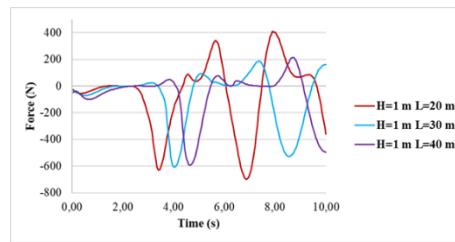
(b)



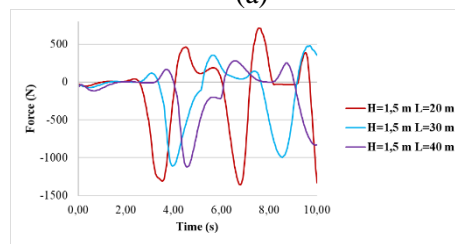
(c)

**Figure 9.** Torque value on turbine blades due to time-dependent wave at fixed wavelength a) Wave heights ( $H$ ) are 1 m, 1.5 m and 2 m and wavelength ( $L$ ) is 20 m b) Wave heights ( $H$ ) are 1 m, 1.5 m and 2 m and wavelength ( $L$ ) is 30 m c) Wave heights ( $H$ ) are 1 m, 1.5 m and 2 m, and wavelength ( $L$ ) is 40 m

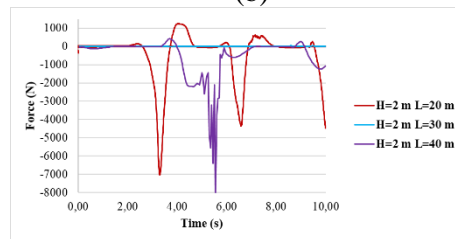
The force value of the wave acting on the turbine blades is presented in Figure 10. Depending on the direction of the wave force, the turbine forces can be positive or negative. The force value of the turbine seemed to change in the same wave profile at wave heights of 1 m and 1.5 m, whereas a force of 8000 N occurs at a wave height of 2 m. At a wave height of 2 m and a wavelength of 30 m, the force value of the turbine goes to zero during the measurement. The figure presents the average force on the turbine blades, which becomes zero due to the bidirectional force effect on the turbine blade in this region, despite the rotational movement caused by the increase in wavelength. The force on the turbine blades remains constant with wavelength, but a time delay occurs due to the change in period.



(a)



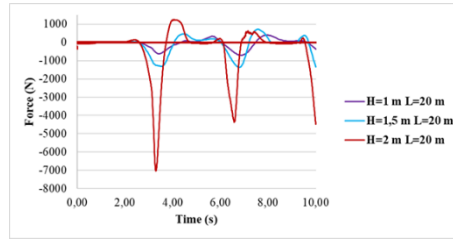
(b)



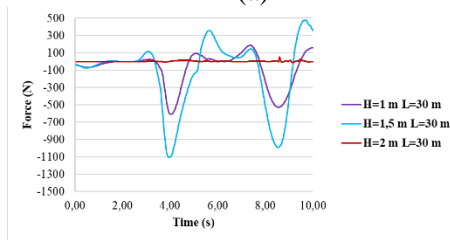
(c)

**Figure 10.** Force value on turbine blades due to time-dependent wave at standing wave height a) Wave height ( $H$ ) is 1 m, and wavelengths ( $L$ ) are 20 m, 30 m and 40 m. b) Wave height ( $H$ ) is 1.5 m, and wavelengths ( $L$ ) are 20 m, 30 m and 40 m. c) Wave height ( $H$ ) is 2 m, and wavelengths ( $L$ ) are 20 m, 30 m and 40 m

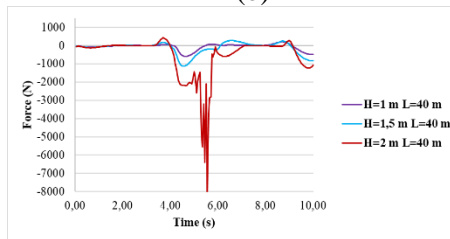
Figure 11 illustrates the change in the force value over time as a function of wave height at a fixed wavelength. As depicted in Figure 10.a, the wave height increases approximately 8 times at around 0.5 m. The force value variation in the turbine for a wave height of 2 m and a wavelength of 20 m changes in the same time step as for wavelengths of 1 m and 1.5 m. However, deformation is observed in 30 m and 40 m wavelengths due to the strain that occurs in the turbine's rotation, in contrast to other values.



(a)



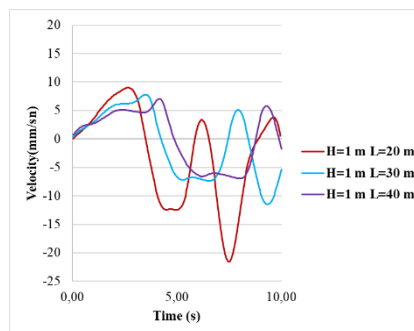
(b)



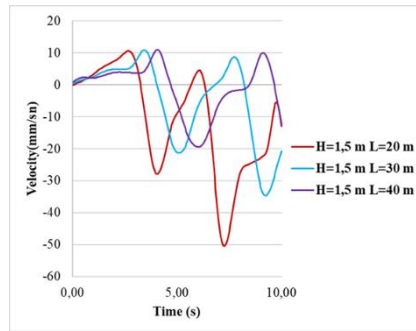
(c)

**Figure 11.** Force value on turbine blades due to time-dependent wave at fixed wavelength a) Wave heights ( $H$ ) are 1 m, 1.5 m and 2 m and wavelength ( $L$ ) is 20 m b) Wave heights ( $H$ ) are 1 m, 1.5 m and 2 m and wavelength ( $L$ ) is 30 m. c) Wave heights ( $H$ ) are 1 m, 1.5 m and 2 m, and wavelength ( $L$ ) is 30 m

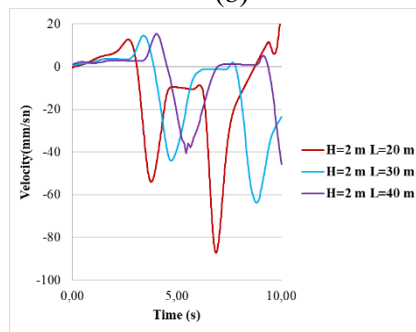
Figure 12 shows the turbine rotation speed as a function of time for all nine wave types. The results revealed that the turbine undergoes rotational motion for all wave types. Furthermore, the turbine rotation speed increases with an increase in wave height. The maximum turbine speed was attained for a wave height of 2 m and a wavelength of 20 m, reaching 87 mm/sec. However, the turbine speed decreased as the wavelength increased for wave heights of 1 m, 1.5 m, and 2 m.



(a)



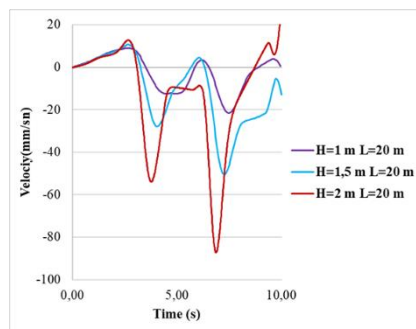
(b)



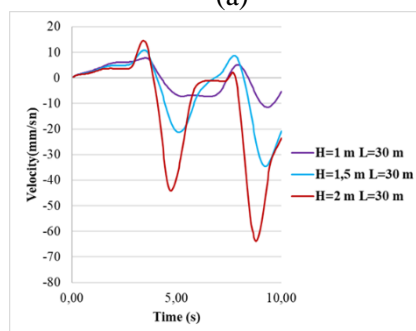
(c)

**Figure 12.** The velocity of turbine shaft due to time-dependent wave at standing wave height a) Wave height ( $H$ ) is 1 m, and wavelengths ( $L$ ) are 20 m, 30 m and 40 m. b) Wave height ( $H$ ) is 1.5 m, and wavelengths ( $L$ ) are 20 m, 30 m and 40 m. c) Wave height ( $H$ ) is 2 m, and wavelengths ( $L$ ) is 20 m, 30 m and 40 m

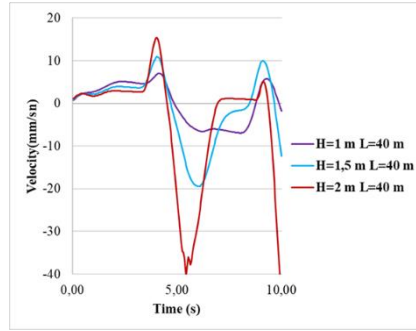
Figure 13 displays the dependence of the turbine shaft speed on various wave heights at a fixed wavelength. The results indicated that the turbine shaft speed increases at the minimum wavelength of 40 m. At a wave height of 2 m, a speed of 40 mm/sec was achieved.



(a)



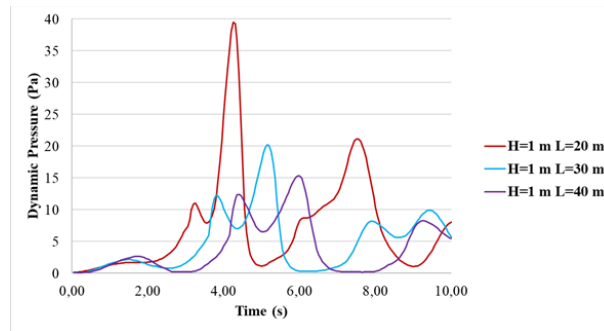
(b)



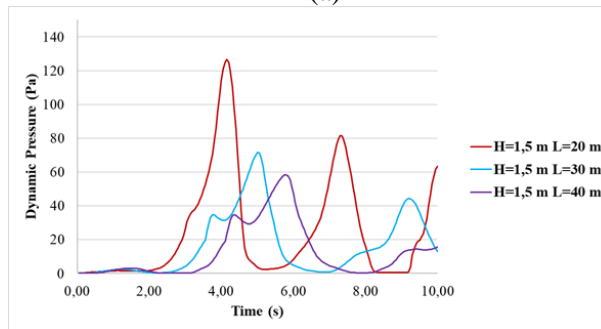
(c)

**Figure 13.** The velocity of turbine shaft due to time-dependent wave at fixed wavelength a) Wave heights ( $H$ ) are 1 m, 1.5 m and 2 m, and wavelength ( $L$ ) is 20 m. b) Wave heights ( $H$ ) are 1 m, 1.5 m and 2 m and wavelength ( $L$ ) is 30 m. b) Wave heights ( $H$ ) are 1 m, 1.5 m and 2 m, and wavelength ( $L$ ) is 40 m

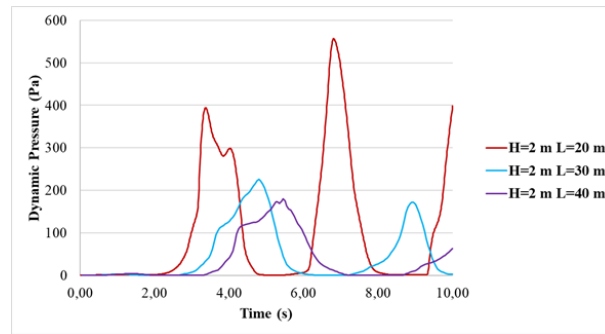
Figure 14 illustrates the dynamic pressure on the turbine blades as a function of time. Dynamic pressure is generated due to the fluid velocity. As the wavelength increases, the wave period also increases, resulting in a decrease in the frequency of the wave. Conversely, low wavelength waves have a higher frequency. Figure 13 shows that the dynamic pressure is higher at a wavelength of 20 m as the wave period increases. In Figure 14.(a), the dynamic pressure value approaches 40 Pa at a wavelength of 20 m, and this value is obtained at 20 Pa for a wavelength of 30 m. However, the pressure drops to 15 Pa at a wavelength of 40 m.



(a)



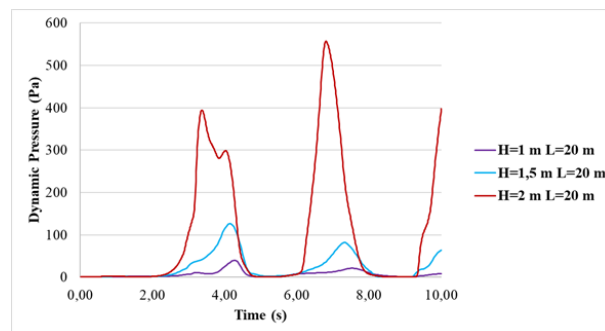
(b)



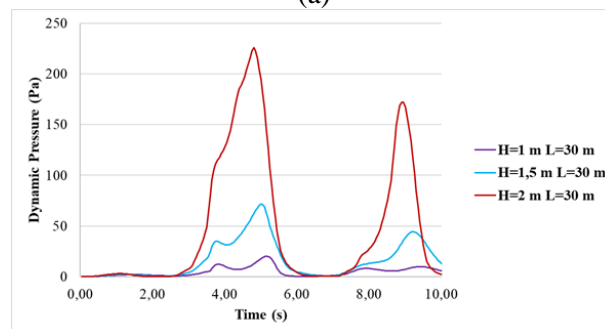
(c)

**Figure 14.** Dynamic pressure due to time-dependent wave at standing wave height a) Wave height ( $H$ ) is 1 m, and wavelengths ( $L$ ) are 20 m, 30 m and 40 m. b) Wave height ( $H$ ) is 1.5 m, and wavelengths ( $L$ ) are 20 m, 30 m and 40 m. c) Wave height ( $H$ ) is 2 m, and wavelengths ( $L$ ) are 20 m, 30 m and 40 m

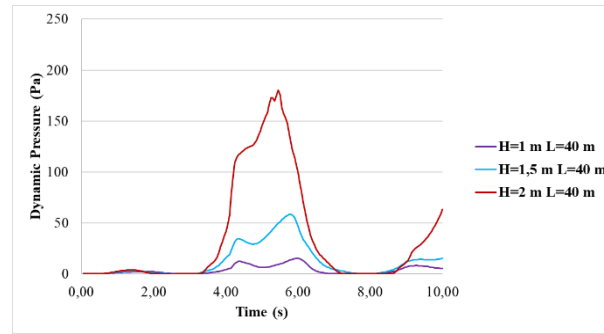
Figure 15 illustrates the absolute dynamic pressure value of the turbine blades at a fixed wavelength as the wave height changes. The study found that the highest dynamic pressure value of 557 Pa occurred at a wave height of 2 m and a wavelength of 20 m. However, a significant decrease was observed in the dynamic pressure value at a wave height of 1.5 m, which resulted in a dynamic pressure of 126 Pa. At a wave height of 1 m, the dynamic pressure value dropped even further to 40 Pa. In Figure 14.b, the dynamic pressure value on the turbine blades was examined for a standing wave height of 30 m. The study found that the maximum dynamic pressure value of 557 Pa occurred at a wavelength of 20 m, with the maximum dynamic pressure decreasing to 226 Pa at a wave height of 30 m. Further, at a wave height of 40 m, the dynamic pressure value dropped to 172 Pa.



(a)



(b)



(c)

**Figure 15.** Dynamic pressure due to time-dependent wave at fixed wavelength a) Wave heights ( $H$ ) are 1 m, 1.5 m and 2 m, and wavelength ( $L$ ) is 20 m. b) Wave heights ( $H$ ) are 1 m, 1.5 m and 2 m and wavelength ( $L$ ) is 30 m. c) Wave heights ( $H$ ) are 1 m, 1.5 m and 2 m, and wavelength ( $L$ ) is 40 m.

The turbine plays a vital role in absorbing the wave power, which is calculated using Equations (2), (3) and provided in Table 1. As the wave height increases, so does the power of the wave, with the maximum power obtained at a wave height of 1 cm and a wave period of 8.75 s. To absorb the mechanical energy of the wave, it is critical to maintain continuity in the turbine's rotational motion. However, continuity cannot be achieved when the wave period is 10 s, resulting in low efficiency. Similarly, a wave height of 2 cm and wave period of 7 s also result in low efficiency, indicating that as the wave height increases, the turbine's period must also increase to maintain continuity in the rotational speed.

**Table 1.** Wave and turbine power depending on the waveform

Wave Height( $H$ )	Wave Period (T)	$P_0$ (kW)	P(kW)	Efficiency ( $P_0/P$ )*100
1	7	0.14	3.34	4.19
1	8.75	0.80	4.17	19.18
1	10	0.05	4.77	1.05
1.5	7	0.52	7.52	6.91
1.5	8.75	0.26	9.40	2.76
1.5	10	0.12	10.74	1.11
2	7	0.10	13.37	0.74
2	8.75	0.60	16.71	3.60
2	10	0.31	19.10	1.62

#### 4. DISCUSSIONS

The study involves modeling a 3D NWT to investigate the impact of waves on turbine motion. Regular waves of varying heights and wavelengths are generated using the Ansys Fluent VOF model in a wave tank, resulting in nine different wave types. The study analyzes the turbine blade force, momentum, speed, and dynamic pressure as they vary with wave height and wavelength. The results indicated that both the dynamic pressure and torque values decreased with higher wavelength and shorter wave period, whereas turbine speed decreased with higher wavelength. The average force on the turbine blades is affected by the higher wavelength, and a phase angle occurred depending on the wave period. An increase in wave height led to higher average dynamic pressure, turbine speed, force, and moment values on the turbine blades.

In the results, although the maximum turbine speed is obtained at a wave height of 2 m and a wave period of 7 s, the maximum power is obtained in the wave form with a wave height of 1 m and a wave period of 8.75 s because the turbine needs a continuous rotation speed to absorb the power of the wave. In this study, results are obtained for a single turbine geometry. In future studies, results will be obtained for turbines with different geometries to determine the appropriate turbine geometry for each wave form.

#### CONFLICTS OF INTEREST

No conflict of interest was declared by the authors.

**REFERENCES**

- [1] Koca, A., Karakose, P., and Yamaç, H. İ., “Offshore Wave Energy Converter Systems”, 1<sup>st</sup> International Symposium on Graduate Research in Science Focus on Entrepreneurship and Innovation (ISGRS 2018), 73 (özet), (2018).
- [2] Bilgic, I., “Power optimisation of a wave energy converter system”, Master thesis, Mustafa Kemal University, Hatay, (2011).
- [3] Zhi, D., and Zhan, J.-m., “Numerical modeling of wave evolution and runup in shallow water”, *Journal of Hydrodynamics*, 21(6): 731-738, (2009).
- [4] Finnegan, W., and Goggins, J., “Linear irregular wave generation in a numerical wave tank”, *Applied Ocean Research*, 52: 188-200, (2015).
- [5] Zhu, Y., Li, Y., Tao, A., and Zhang, J., “Numerical modeling of wave interaction with double curtain-wall breakwater”, *Procedia Engineering*, 116(2015): 1009-1018, (2015).
- [6] Ojieh, N., Barltrop, N., and Xu, L., “Rans investigation of the kinematics of an alternative extreme wave”, *Ocean engineering*, 36(17-18): 1415-1424, (2009).
- [7] Liu, T.-L., and Lin, C.-C., “Wave-maker stroke design and wave decay methods in numerical wave tank study”, *J CCIT*, 41: 101-106, (2012).
- [8] Wu, N.-J., Tsay, T.-K., and Chen, Y.-Y., “Generation of stable solitary waves by a piston-type wave maker”, *Wave Motion*, 51(2): 240-255, (2014).
- [9] Saincher, S., and Banerjee, J., “Design of a numerical wave tank and wave flume for low steepness waves in deep and intermediate water”, *Procedia Engineering*, 116: 221-228, (2015).
- [10] Yamaç, H. İ., Koca, A., and Yılmaz, T., “Using computational fluid dynamics for wave generation and evaluation of results in numerical wave tank modelling”, *Firat University Journal of Experimental and Computational Engineering*, 1(1): 31-42, (2022).
- [11] Yamaç, H. İ., and Koca, A., “Numerical analysis of wave energy converting systems in case of using piezoelectric materials for energy harvesting”, *Journal of Marine Engineering & Technology*, 20(2): 138-149, (2022).
- [12] Yamac, H., “Modeling and analysis of the wave energy converting systems in case of using piezoelectric materials for harvesting energy”, Master Thesis, Firat University, Elazig, (2016).
- [13] Liu, J.-Q., Fang, H.-B., Xu, Z.-Y., Mao, X.-H., Shen, X.-C., Chen, D., Liao, H., and Cai, B.-C., “A mems-based piezoelectric power generator array for vibration energy harvesting”, *Microelectronics Journal*, 39(5): 802-806, (2008).
- [14] Bhinder, M. A., Babarit, A., Gentaz, L., and Ferrant, P., “Potential time domain model with viscous correction and cfd analysis of a generic surging floating wave energy converter”, *International Journal of Marine Energy*, 10: 70-96, (2015).
- [15] Yamaç, H. İ., Koca, A., and Karakose, P., " Numerical Analysis of Wave Amplitude Effect on Power Output of Oscillating Water Column Device with Coastal Elevation", 1st International Engineering and Technology Symposium (IETS'18), 208-211, (2018).
- [16] Koca, A., and Yamaç, H. İ., “Oscillating Water Column Analysis in Numerical Wave Tank with

- Variable Base Geometries”, International Advanced Researches & Engineering Congress 2017 Proceeding Book, (2017).
- [17] Anbarsooz, M., Faramarzi, A., and Ghasemi, A., “A numerical study on the performance of fixed oscillating water column wave energy converter at steep waves”, in ASME power conference, American Society of Mechanical Engineers, 50213, V001T08A003, (2016).
- [18] Gomes, M. D. N., Nascimento, C. D. D., Bonafini, B. L., Santos, E. D. D., Isoldi, L. A., and Rocha, L. A. O., “Two-dimensional geometric optimization of an oscillating water column converter in laboratory scale”, *Revista de Engenharia Térmica*, 11(1-2): 30-36, (2012).
- [19] Morris, C. E., O'Doherty, D. M., O'Doherty, T., and Mason-Jones, A., “Kinetic energy extraction of a tidal stream turbine and its sensitivity to structural stiffness attenuation”, *Renewable Energy*, 88: 30-39, (2016).
- [20] Sarma, N., Biswas, A., and Misra, R., “Experimental and computational evaluation of savonius hydrokinetic turbine for low velocity condition with comparison to savonius wind turbine at the same input power”, *Energy Conversion and Management*, 83: 88-98, (2014).
- [21] Kumar, A., Saini, R., “Performance analysis of a single-stage modified savonius hydrokinetic turbine having twisted blades”, *Renewable Energy*, 113: 461-478, (2017).
- [22] Elbatran, A., Ahmed, Y. M., and Shehata, A. S., “Performance study of ducted nozzle savonius water turbine, comparison with conventional savonius türbine”, *Energy*, 134: 566-584, (2017).
- [23] Bai, G., Li, W., Chang, H., and Li, G., “The effect of tidal current directions on the optimal design and hydrodynamic performance of a three-turbine system”, *Renewable Energy*, 94: 48-54, (2014).
- [24] McCormick, M. E., “Ocean engineering mechanics: with applications”, Cambridge University Press, (2009).
- [25] Dalrymple, R. A., and Dean, R. G., “Water wave mechanics for engineers and scientists”, World Scientific Publishing Company, 2, (1991).